Ursa Major III/UNIONS 1: The Darkest Galaxy Ever Discovered?

Raphaël Errani, Julio F Navarro, Simon E.T Smith, Alan W Mcconnachie

The Astrophysical Journal, 965:20 (11pp), 2024 April 10 https://doi.org/10.3847/1538-4357/ad2267

Ursa Major III/UNIONS 1: The Darkest Galaxy Ever Discovered?

Raphaël Errani[1,2], Julio F. Navarro[3], Simon E. T. Smith[3], and Alan W. McConnachie[4,3]
[1] McWilliams Center for Cosmology, Department of Physics, Carnegie Mellon University, Pittsburgh, PA 15213, USA; errani@cmu.edu
[2] Université de Strasbourg, CNRS, Observatoire Astronomique de Strasbourg, UMR 7550, F-67000 Strasbourg, France
[3] Department of Physics and Astronomy, University of Victoria, Victoria, BC, V8P 5C2, Canada
[4] NRC Herzberg Astronomy and Astrophysics, 5071 West Saanich Road, Victoria, BC, V9E 2E7, Canada
Received 2023 October 30; revised 2024 January 7; accepted 2024 January 23; published 2024 April 2

Abstract

The recently discovered stellar system Ursa Major III/UNIONS 1 (UMa3/U1) is the faintest known Milky Way satellite to date. With a stellar mass of $16^{+6}_{-5}\,M_\odot$ and a half-light radius of 3 ± 1 pc, it is either the darkest galaxy ever discovered or the faintest self-gravitating star cluster known to orbit the Galaxy. Its line-of-sight velocity dispersion suggests the presence of dark matter, although current measurements are inconclusive because of the unknown contribution to the dispersion of potential binary stars. We use *N*-body simulations to show that, if self-gravitating, the system could not survive in the Milky Way tidal field for much longer than a single orbit (roughly 0.4 Gyr), which strongly suggests that the system is stabilized by the presence of large amounts of dark matter. If UMa3/U1 formed at the center of a $\sim 10^9\,M_\odot$ cuspy LCDM halo, its velocity dispersion would be predicted to be of order ~ 1 km s^{-1}. This is roughly consistent with the current estimate, which, neglecting binaries, places $\sigma_{\rm los}$ in the range 1–4 km s^{-1}. Because of its dense cusp, such a halo should be able to survive the Milky Way tidal field, keeping UMa3/U1 relatively unscathed until the present time. This implies that UMa3/U1 is plausibly the faintest and densest dwarf galaxy satellite of the Milky Way, with important implications for alternative dark matter models and for the minimum halo mass threshold for luminous galaxy formation in the LCDM cosmology. Our results call for multi-epoch high-resolution spectroscopic follow-up to confirm the dark matter content of this extraordinary system.

Unified Astronomy Thesaurus concepts: Cold dark matter (265); Dwarf spheroidal galaxies (420); Low surface brightness galaxies (940); the Milky Way (1054); N-body simulations (1083); Star clusters (1567); Tidal disruption (1696)

1. Introduction

Ultrafaint dwarf galaxies (UFDs) are stellar systems with $M_\star < 10^5\,M_\odot$, fainter than many globular clusters (GCs) but gravitationally bound by the presence of large amounts of dark matter. They constitute direct probes not only of the formation mechanisms that govern the extreme faint end of the galaxy luminosity function, but also of the structure of low-mass dark matter halos and, indirectly, of the nature of dark matter (see, e.g., Bullock & Boylan-Kolchin 2017; Simon 2019; Sales et al. 2022, for recent reviews).

The overall abundance of UFDs reflects the number of low-mass dark matter halos able to harbor luminous galaxies, placing important constraints on models where the physical nature of dark matter leads to the suppression of low-mass halos, such as in "warm dark matter" (Bode et al. 2001; Lovell et al. 2014) or "fuzzy dark matter" (FDM; e.g., Hu et al. 2000) models. For cold dark matter (CDM) models, where the number of low-mass halos is expected to be overwhelmingly larger than the number of UFDs, the abundance of faint systems probes the mass threshold between halos that remain "dark" (starless) and those massive enough for luminous galaxy formation to proceed (Simon & Geha 2007; Ferrero et al. 2012; Peñarrubia et al. 2012; Fattahi et al. 2018).

This threshold is still being actively discussed, with some studies suggesting a relatively high virial[5] halo mass threshold ($\sim 10^9\,M_\odot$; Benitez-Llambay & Frenk 2020; Pereira-Wilson et al. 2023), determined primarily by the ability of hydrogen to cool in halos photoheated by the ambient UV background (Efstathiou 1992; Quinn et al. 1996; Gnedin 2000), and other studies arguing for a much lower mass threshold, in order to accommodate the sheer number of observed UFDs plus those still likely missing from our currently incomplete inventory of Milky Way satellites (e.g., Nadler et al. 2021 and references therein).

In addition, because UFDs are physically small and heavily dark-matter-dominated, they probe the innermost regions of their dark matter halos, where competing dark matter models make differing predictions. CDM models predict "cuspy" density profiles (Navarro et al. 1996, 1997), which imply high average dark matter densities for UFDs. Cuspy halos are remarkably resilient to tidal stripping (Peñarrubia et al. 2008, 2010; Amorisco 2021; Errani & Navarro 2021, hereafter EN21) and may host "microgalaxies," even after undergoing substantial tidal mass loss (Errani & Peñarrubia 2020, hereafter, EP20).

On the other hand, self-interacting dark matter (SIDM) or FDM models generally predict much lower dark matter densities, as a result of the inward energy transfer driven by self-interactions (SIDM—Colín et al. 2002; Zavala et al. 2013;

[5] Virial quantities are identified by a "200" subscript and defined at or within the virial radius, r_{200}, which encloses a mass mean average density equal to 200 times the critical density for closure. At $z = 0$, $\rho_{\rm crit} = 3H_0^2/(8\pi G)$, with $H_0 = 67$ km s^{-1} Mpc^{-1} (Planck Collaboration et al. 2020).

Tulin & Yu 2018) or of the quantum pressure support arising from the uncertainty principle (FDM—Goodman 2000; Hu et al. 2000; Burkert 2020; Ferreira 2021).

Available data indicate that UFDs are, indeed, quite dense (see, e.g., Simon 2019; Battaglia & Nipoti 2022). This result has led recent SIDM modeling to consider much higher interaction cross sections than envisioned in earlier work (Silverman et al. 2023), in an attempt to reconcile observations with SIDM halos whose inner densities have been gravothermally enhanced by "core collapse" (Balberg et al. 2002; Nishikawa et al. 2020; Turner et al. 2021; Correa et al. 2022; Zeng et al. 2022, 2023). The same result places strong constraints on FDM models, too, and suggests that earlier lower-mass bounds for ultralight particles based on the "classical" dwarf spheroidal satellites of the Milky Way should be drastically revised (Safarzadeh & Spergel 2020).

Finally, UFDs are ideal laboratories for studying in unprecented detail the heavy element enrichment process driven by recurring episodes of star formation. Some of these galaxies are so faint and so metal-poor that the abundance pattern of individual stars may well reveal the nucleosynthetic yields of individual Population III supernovae or other explosive stellar events in these chemically pristine systems (Frebel & Norris 2015; Hansen et al. 2017; Ji et al. 2019; Marshall et al. 2019).

These traits make UFDs highly valuable, and have given impetus to a number of specialized UFD searches using resolved stars in widefield photometric surveys. Because they are so faint, UFDs are elusive objects that barely stand out against the foreground of Galactic stars and the background of distant galaxies.

UFD candidates are typically identified by matched-filter techniques, which pinpoint clumps of old stars at a common distance (Koposov et al. 2008; Walsh et al. 2009; Martin et al. 2013; Drlica-Wagner et al. 2015). These clumps are then followed up with deeper photometry and spectroscopy to enable a full characterization of the system. When available, proper motions from the Gaia mission (Simon 2018; Pace & Li 2019; McConnachie & Venn 2020a, 2020b; Li et al. 2021) can help to aid the discovery process, but at the expense of being applicable only to relatively nearby systems, given Gaia's relatively shallow depth compared to contemporary widefield, digital photometric surveys.

Distinguishing dark-matter-dominated UFDs from self-gravitating faint star clusters is the final, perhaps most difficult hurdle, one that can only be fully overcome by securing multi-epoch line-of-sight velocities to test whether the system is a self-gravitating star cluster or a UFD bound by the presence of dark matter (Willman & Strader 2012).

For the faintest and most distant candidates, this is a most challenging task, given the few stars bright enough to obtain spectra for, the limited precision of the individual radial velocities, the uncertainties from low-number statistics (Laporte et al. 2019), and the possibility that binary stars may lead to inflated values of the velocity dispersion, confusing the interpretation (McConnachie & Côté 2010; Minor et al. 2010).

Although a few dozen candidate[6] UFDs are currently known, with total luminosities in the range $+1 > M_V > -3$ and sizes in the range 1–20 pc (e.g., Muñoz et al. 2012; Balbinot et al. 2013; Torrealba et al. 2019; Mau et al. 2020; Cerny et al. 2023b, 2023a), very few of those have been conclusively identified as dark-matter-dominated UFDs because of the difficulties listed above.

The most singular of these candidates is Ursa Major III/UNIONS 1 (hereafter UMa3/U1), an astonishingly faint ($M_V \sim +2.2$) stellar system with a projected half-light radius of only $R_h = 3 \pm 1$ pc recently discovered by Smith et al. (2024, hereafter S24). UMa3/U1 orbits the Milky Way on an inclined, "halo-like" orbit with pericenter $r_{peri} \approx 13$ kpc and apocenter $r_{apo} \approx 30$ kpc. Although comparable in size to GCs, it is ∼10 times fainter than the faintest known GC to date (Inman & Carney 1987; Koposov et al. 2007). It is also at least ∼10 times fainter and ∼five times smaller than the faintest confirmed UFDs (Belokurov et al. 2009; Geha et al. 2009; Martin et al. 2016).

S24 report a velocity dispersion for UMa3/U1 of $\sigma_{los} = 3.7^{+1.4}_{-1.0}$ km s^{-1} on the basis of 11 likely member stars, which would imply a mass-to-light ratio of several thousands. The authors do, however, caution that the estimate of σ_{los} is very sensitive to the inclusion (or exclusion) of specific member stars: removing a single star (the largest outlier in velocity, perhaps a binary star) drops the estimate to $\sigma_{los} = 1.9^{+1.4}_{-1.1}$ km s^{-1}. Removing a second outlier from the sample results in a formally unresolved velocity dispersion, consistent with the extremely small value expected if UMa3/U1 were a self-gravitating star cluster ($\sigma_{los} \sim 50$ m s^{-1}). Should σ_{los} prove much higher than this value, it would imply that UMa3/U1 is the faintest, or "darkest," galaxy ever discovered.

Because of the sensitivity of the σ_{los} estimate to the two outliers, and because of the lack of repeat velocity measurements (needed to rule out the undue influence of binary stars), S24 are unable to ascertain the true nature of UMa3/U1. It is clear, however, that regardless of its nature, this system is truly exceptional.

We present here a simple argument in favor of the interpretation of UMa3/U1 as a genuine dark-matter-dominated UFD. The argument relies on the fact that should UMa3/U1 be a self-gravitating star cluster lacking dark matter, its average density would be comparable to the mean density of the Galaxy at the pericenter of its orbit. As such, it could not survive long on its current orbit, which, given the short orbital time of UMa3/U1 around the Galaxy, seems extremely unlikely.

We elaborate on this idea in Section 2, where we use *N*-body simulations to model the tidal evolution of UMa3/U1, under the assumption that it is a self-gravitating star cluster. In Section 3, we model UMa3/U1 as a dark-matter-dominated *microgalaxy* and show that its estimated velocity dispersion is consistent with that expected if UMa3/U1 inhabits a cuspy $\sim 10^9\, M_\odot$ CDM halo. Finally, we summarize and discuss our main conclusions in Section 4.

2. Self-Gravitating (SG) Model

Assuming that UMa3/U1 is a self-gravitating star cluster, we adopt a simple model where its density profile is approximated by a spherical exponential distribution,

$$\rho_\star(r) = \rho_0 \exp(-r/r_\star)\,, \tag{1}$$

with a scale radius $r_\star$ and a total stellar mass $M_\star = 8\pi\, \rho_0\, r_\star^3$. The 3D and 2D half-mass radii are related to the scale radius through $r_h \approx 2.67\, r_\star$ and $R_h \approx 2.02\, r_\star$, respectively. Under the

[6] We colloquially refer to these systems as "glorfs"—i.e., either a dwarf galaxy or a GC.

assumption of dynamical equilibrium, the line-of-sight velocity dispersion may be computed from the projected virial theorem (Amorisco & Evans 2012; Errani et al. 2018):

$$\langle \sigma_{\rm los}^2 \rangle = \frac{5}{96}\frac{GM_\star}{r_\star}\,. \tag{2}$$

Using the parameters estimated by S24, $M_\star = 16^{+6}_{-5}\,M_\odot$ and $R_{\rm h} = (3 \pm 1)$pc, we estimate, for the self-gravitating case, a line-of-sight velocity dispersion of

$$\sigma_{\rm los} \equiv \langle \sigma_{\rm los}^2 \rangle^{1/2} = 49^{+14}_{-11}\ {\rm m\ s^{-1}}\,. \tag{3}$$

The uncertainties above are estimated from a Monte Carlo sample, taking into account the asymmetric measurement uncertainties on $M_\star$ and $R_{\rm h}$. Note that a velocity dispersion this small is well below what S24 could measure, given their observational setup.

Confirming that the (virial) velocity dispersion of UMa3/U1 is indeed of the order of a few kilometers per second, as suggested from the dispersion estimate of S24 from the 10- and 11-member samples (see Section 1), would rule out conclusively and convincingly the possibility that this system is a self-gravitating star cluster.

2.1. Tidal Evolution

2.1.1. N-body Models

We use N-body simulations to analyze the evolution of the SG UMa3/U1 model described above in the Milky Way gravitational potential. With a total stellar mass of $M_\star = 16^{+6}_{-5}\,M_\odot$, UMa3/U1 likely contains only a few dozen stars (S24 estimate $N_\star \sim 21^{+6}_{-5}$ stars brighter than 23.5 mag). The system is therefore intrinsically *collisional*, giving rise to a complex internal dynamical evolution that depends on the initial stellar mass function, the fraction of binary stars, the number of potential stellar remnants like neutron stars and black holes, and the exact stochastic realization of the underlying distribution function. None of these initial properties are well understood for faint stellar systems. A full exploration of this parameter space is hence, at the present day, impractical at best. With these caveats in mind, we model in this section UMa3/U1 as a *collisionless* system, which should be enough to broadly illustrate the dynamical evolution of UMa3/U1 in the Milky Way potential.

The progenitor of UMa3/U1 is modeled as an N-body realization of an exponential sphere with 10^6 particles with isotropic velocity dispersion, generated using the code described in EP20, available online.[7] We explore models with initial masses in the range $16 \leqslant M_\star/M_\odot \leqslant 160$. All models have the same initial (2D) half-light radius of $R_{\rm h} = 3$ pc.

For the Milky Way halo, we assume the static, analytical potential from EP20. The potential includes a thick and a thin axisymmetric Miyamoto & Nagai (1975) disk ($M_{\rm thick} = 2.0 \times 10^{10}\,M_\odot$, $M_{\rm thin} = 5.9 \times 10^{10}\,M_\odot$, radial scale lengths $a_{\rm thick} = 4.4$ kpc, $a_{\rm thin} = 3.9$ kpc, and vertical scale lengths $b_{\rm thick} = 0.92$ kpc, $b_{\rm thin} = 0.31$ kpc for the thick and thin disk, respectively), a spherical Hernquist (1990) bulge ($M_{\rm b} = 2.1 \times 10^{10}\,M_\odot$ and scale length $a_{\rm b} = 1.3$ kpc), and a Navarro–Frenk–White (NFW; Navarro et al. 1996, 1997) dark matter halo ($M_{200} = 1.15 \times 10^{12}\,M_\odot$, $r_{200} = 192$ kpc, and concentration $c = 9.5$), with parameters chosen to approximate the circular velocity curve of McMillan (2011). In practice, the adopted Galactic potential is not too different, in the regions of interest, from that of a singular isothermal sphere with constant circular velocity, $V_{\rm c} \approx 240\ {\rm km\ s^{-1}}$. See Appendix A for a wider exploration of potentials and orbits.

The integration is performed using the particle mesh code SUPERBOX (Fellhauer et al. 2000). This code employs two cubic grids of 128^3 cells comoving with the N-body model with resolutions of 0.04 and 0.4 pc, respectively, as well as a fixed 128^3 cell grid containing the entire simulation volume, with a lower resolution of ≈1.6 kpc.

2.1.2. Tidal Disruption Timescales

We begin by simply evolving the SG UMa3/U1 model forward from its observed present-day position and proper motions, as listed by S24. Using the Schönrich et al. (2010) solar velocity with respect to the local standard of rest results in an orbit with a pericenter of $r_{\rm peri} \approx 13$ kpc and apocenter of $r_{\rm apo} \approx 30$ kpc. The total bound mass is shown, as a function of time, in Figure 1, where the blue diamond symbol (along the vertical dotted line labeled "now") represents the present-day configuration of UMa3/U1. As is clear from this figure, the system fully disrupts in less than two radial orbital times (with $T_{\rm orb} = 0.4$ Gyr in the EP20 potential). This result holds for all orbits compatible with the observed position and velocity of UMa3/U1; see Appendix A.

The short survival time of the SG UMa3/U1 model is not surprising, for its mean density is comparable to the mean density of the Milky Way inside the pericenter of the orbit:

$$\bar{\rho}_{\rm peri} = 3\big/(4\pi G)\,(V_{\rm peri}^2/r_{\rm peri}^2) \approx 1.9 \times 10^7\,M_\odot\ {\rm kpc^{-3}}, \tag{4}$$

where $V_{\rm peri} \approx 240\ {\rm km\ s^{-1}}$ (Huang et al. 2016; Eilers et al. 2019) is the circular velocity of the Milky Way at $r_{\rm peri}$. For comparison, the mean density of the SG UMa3/U1 model within its 3D half-light radius is

$$\bar{\rho}_{\star {\rm h}} = 3\,M_\star/(8\pi r_{\rm h}^3) = 2.9^{+7.2}_{-1.8} \times 10^7\,M_\odot\ {\rm kpc^{-3}}, \tag{5}$$

where the quoted uncertainty takes into account the asymmetric measurement uncertainties on stellar mass $M_\star$ and half-light radius.

To complete the analysis, we modify the initial mass of the SG UMa3/U1 model to ensure that it survives for a longer period of time on the same orbit, and adjust it to match, at present, the observed properties of UMa3/U1. The initial conditions are generated by first integrating the orbit backward in time. For the model to match today's properties after evolving for, say, 12 Gyr (i.e., ∼27 full orbits), it must have been substantially more massive/denser, as indicated by the red diamond symbol in Figure 1. Tidal mass loss little affects the size of the bound remnant, so a model with a similar half-mass radius but an initial mass of $\sim 136\,M_\odot$ could, in principle, have been the progenitor of today's UMa3/U1. The evolution of this progenitor in the mass–radius plane is shown in Figure 2.

The colored curves in Figure 2 are fitted to the disruption times measured in the simulations. As shown in Errani et al. (2023), on a given orbit, the disruption times depend mainly on the initial density contrast between the progenitor and host, measured at pericenter. Intermediate values of the initial mass (i.e., in the range $16 \leqslant M_\star/M_\odot \leqslant 160$) lead, as expected, to

[7] https://github.com/rerrani/nbopy

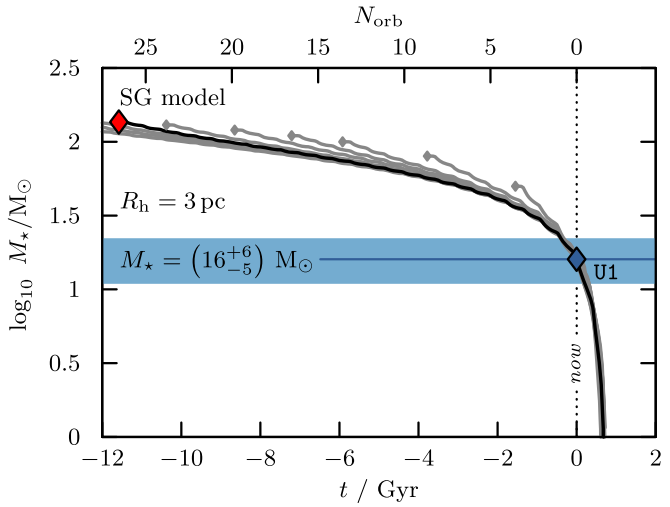

Figure 1. Mass evolution of self-gravitating (SG) N-body models for the UMa3/U1 stellar system. All models have an initial (2D) half-light radius of $R_{\rm h} = 3$ pc. A blue band shows the 1σ measurement uncertainty around the current mass of UMa3/U1. The evolution of an example model with initial mass $M_\star = 136\,M_\odot$ (the red diamond symbol) is highlighted in black . Note that all models, independently of their initial mass, fully disrupt within ~0.6 Gyr from now, suggesting that if UMa3/U1 is a self-gravitating object, then we observe it at a very special point in time in its evolution.

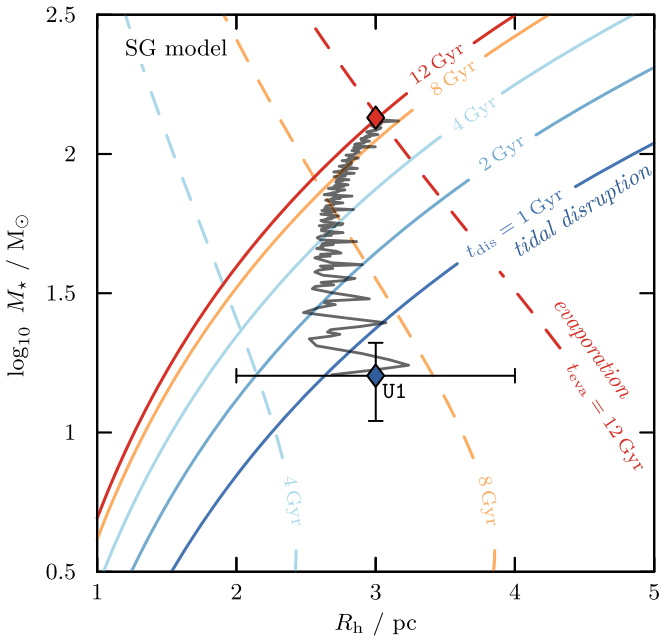

Figure 2. The same as Figure 1, but for the tidal evolution in the mass–size plane. Numerical estimates of the tidal disruption ($t_{\rm dis}$) and evaporation ($t_{\rm eva}$, Equation (7)) timescales are shown by the solid and dashed colored curves, respectively. The present-day mass and size of UMa3/U1 are shown as the blue diamond with 1σ error bars. The gray curve shows the evolution of the example model highlighted in Figure 1.

intermediate survival times, as shown by the gray lines/diamonds in Figure 1. Still, all of these models disrupt fully in less than ~0.6 Gyr from now. Given that stars in UMa3/U1 are likely $\gtrsim$11 Gyr old (S24), it would require quite the coincidence to discover UMa3/U1 just as we witness its final orbit around the Milky Way.

2.1.3. Tidal Debris

However unlikely the SG model of UMa3/U1 might be, a robust prediction that may be scrutinized observationally is the presence of tidal debris along the orbit. Given the extremely low velocity dispersion of the progenitor, the debris should align along a thin stream, as depicted by the red dots in the top panel of Figure 3. The particular realization shown in this figure corresponds to the 12 Gyr old progenitor identified by the red diamond in Figure 1, but the configuration would be similar for other massive progenitors. Note that the N-body model used here approximates UMa3/U1 as a collisionless system. The detailed stream properties will be affected by internal collisional processes, which in turn depend on the initial mass function, the fraction of binary stars, and the presence of dark stellar remnants (see, e.g., Spurzem & Kamlah 2023).

The bottom panel of Figure 3 shows a close-up view of the present-day configuration of the simulated UMa3/U1 system, in Galactic coordinates. Because of the intrinsic faintness of the system, only a few individual stars are expected to trace the tidal tails outside the inner couple of arcminutes from the center of the system (the half-mass radius spans roughly $1'$ at 10 kpc, the assumed distance of UMa3/U1; see S24).

We may use those stars to test the possibility that the velocity dispersion estimate of UMa3/U1 might be artificially enhanced by the presence of stars in the process of being stripped from the system. We find that the line-of-sight velocity dispersion using all stars within 1, 2, 3, and 5 half-mass radii varies by less than $\sim$20 m s^{-1} from its average value of $\sim$60 m s^{-1}. In addition, the total line-of-sight velocity gradient across the galaxy is less than 25 m s^{-1} arcmin^{-1}, so that stars $6'$ ahead or behind the main body of the remnant differ by less than 300 m s^{-1} on average, a value too small to be detectable with the line-of-sight velocities of S24. These results are not unexpected, given the extremely low escape velocity of the SG UMa3/U1 model, which (assuming the exponential profile of Equation (1)) is only $v_{\rm esc} = (GM_\star/r_\star)^{1/2} \approx 215$ m s^{-1} at the center. For comparison, all of the likely UMa3/U1 members with available velocity estimates identified by S24 lie within $4\,R_{\rm h}$ from the center of UMa3/U1.

The velocity dispersion estimate in the SG model thus seems to depend only weakly on the radial extent over which stars are collected, and certainly does not approach in any case the few kilometers per second estimated by S24 using 10 or 11 likely members (and neglecting binaries). We conclude that the inclusion of weakly bound stars, or of stars stirred by the Galactic tidal field, cannot explain such a high velocity dispersion estimate.

2.2. Evaporation Timescales

In addition to external tidal forces, internal collisional processes may alter the structure and bound mass of a stellar system. This is especially true for a system with as few stars as UMa3/U1, which may "evaporate" due to collisions between stars in less than a Hubble time. Assuming, for simplicity, that all stars have the same mass of $\sim$0.25 $M_\odot$, we find that UMa3/U1 has approximately $N_{\rm h} \approx 2\,M_\star/M_\odot \approx 32$ stars within the half-light radius. For an isolated cluster, the relaxation time is related to the half-mass crossing time by (see e.g. Equation (2-62) in Spitzer (1987) and Equation (8-1) in Binney & Tremaine (1987)):

$$T_{\rm rel} \approx \frac{N_{\rm h}}{8\,\ln N_{\rm h}}\,T_{\rm cross} = (48 \pm 25)\ {\rm Myr}\ , \qquad (6)$$

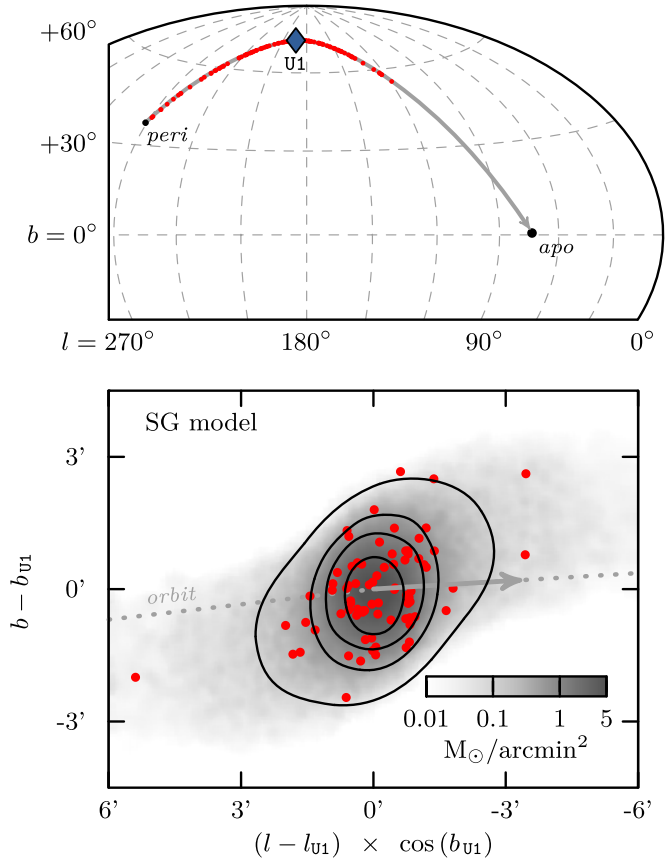

Figure 3. Top panel: orbit of UMa3/U1 in Galactic coordinates. The red points show a Monte Carlo sample of stripped stars drawn from the *N*-body model highlighted in Figure 1. Bottom panel: surface density map of the SG model (grayscale). The orbit is shown using a dotted curve, with an arrow indicating the direction of motion along the orbit.

where $T_{\rm cross} \approx (GM_\star/2r_{\rm h}^3)^{-1/2} = (42 \pm 22)$Myr for $M_\star = 16\,M_\odot$ and $r_{\rm h} = 4$ pc. The uncertainties quoted here are estimated by linear propagation of the measurement uncertainties.

A rough estimate of the evaporation timescale is then given by (see p. 491 in Binney & Tremaine (1987)):

$$T_{\rm evap} \approx 136\,T_{\rm rel} = (6.5 \pm 3.4)\,{\rm Gyr}\,. \quad (7)$$

This timescale is substantially longer than the timescale for full tidal disruption. Evaporation time estimates are shown as the dashed colored curves in Figure 2. Collisional evaporation is thus unlikely to alter our main conclusion above: the short time to full tidal disruption clearly disfavors the suggestion that UMa3/U1 is a self-gravitating star cluster.

3. Dark-matter-dominated Model

The simplest alternative to explain the long-term survival of UMa3/U1 in the Galactic tidal field is that UMa3/U1 is embedded in a dark matter subhalo, which protects the stellar component from tidal forces. The presence of dark matter would lead to a much increased velocity dispersion compared with the self-gravitating case studied in the previous section.

As a definite example, we shall adopt below the 10-member dispersion estimate of $\sigma_{\rm los} = 1.9^{+1.4}_{-1.1}$ km s^{-1} reported by S24, although we note again that this value may be revised once future observations enable a proper accounting of the effect of potential binary stars. We note as well that even a lower value of the velocity dispersion would qualify UMa3/U1 as a UFD, provided that it is substantially above the $\sim$50 m s^{-1} expected from the SG model.

3.1. Dynamical Mass Estimate

The velocity dispersion adopted above would imply a dyamical-to-stellar mass ratio comparable to the most heavily dark-matter-dominated dwarfs known to date. We show this in Figure 4, where we contrast UMa3/U1 with a compilation[8] of dynamical and stellar masses of Local Group dwarf galaxies (squares) and GCs (circles) with measured kinematics. The diagonal dashed curves correspond to constant dynamical-to-stellar mass ratios, approximated by

$$\Upsilon_{\rm dyn} \equiv \frac{M_{\rm dyn}(<r_{\rm h})}{M_\star/2} \approx 8\,R_{\rm h}\,\langle\sigma^2_{\rm los}\rangle\,G^{-1}M_\star^{-1}\,. \quad (8)$$

In the above equation, we estimate the dynamical mass $M_{\rm dyn}(<r_{\rm h})$ enclosed within the 3D half-light radius $r_{\rm h}$ from the combined measurement of the line-of-sight velocity dispersion $\sigma_{\rm los}$ and 2D half-light radius $R_{\rm h}$, with the coefficient[9] as in Wolf et al. (2010) and Errani et al. (2018). The total stellar mass $M_\star$ is approximated assuming a stellar mass-to-light ratio of $M_\star/L_{\rm V} \approx 1.6$ (as in Woo et al. 2008 for galaxies with old stellar populations). Self-gravitating star clusters closely follow a line with constant dynamical-to-stellar mass ratio labeled $\Upsilon_{\rm dyn} = 1$, whereas dwarfs are clearly offset to much higher values of the dynamical-to-stellar mass ratio.

The blue diamond at the bottom left corner shows where UMa3/U1 would be located if it was a faint GC akin to the SG model explored earlier (in which case it would be called "UNIONS 1," or U1, for short). The other blue diamond labeled "UMa3" corresponds to adopting the 10-star dispersion $\sigma_{\rm los} = 1.9^{+1.4}_{-1.1}$ km s^{-1}, resulting in a dynamical-to-stellar mass ratio of $\Upsilon_{\rm dyn} = 1.2^{+2.8}_{-1.0} \times 10^3$. In this case, UMa3 sits comfortably close to the dwarf galaxy trend, extrapolated to extremely low stellar masses (i.e., extremely faint luminosities).

Assuming hereafter that UMa3/U1 is a dwarf galaxy (in which case it would simply be called "Ursa Major III," or UMa3, for short), we examine next whether it would be expected to survive the strong Galactic tidal field. We begin by comparing in Figure 5 the mean density of the system within its half-mass radius, $\bar{\rho}_{\rm h}$, with $\bar{\rho}_{\rm peri}$, the mean density of the Galaxy at the pericenter of the orbit, shown by a horizontal dotted line segment. As discussed earlier, the "U1" symbol indicates that UMa3/U1's density would be comparable to $\bar{\rho}_{\rm peri}$ (and thus doomed to rapid tidal disruption) if it was a self-gravitating cluster.

[8] The data shown for dwarf galaxies are as compiled in McConnachie (2012)—the version from 2021 January, with updated data for Antlia 2 (Ji et al. 2021), Bootes 2 (Bruce et al. 2023), Crater 2 (Ji et al. 2021), Tucana (Taibi et al. 2020), Tucana 2 (Chiti et al. 2021), And 19 (Collins et al. 2020), and And 21 (Collins et al. 2021). For GCs, the data are taken from Harris (1996)—the version from 2010 December, with updated half-light radii and velocity dispersions for Pal-5 from Kuzma et al. (2015) and Gieles et al. (2021), for NGC 2419 from Baumgardt et al. (2009), and for Pal-14 from Hilker (2006) and Jordi et al. (2009).

[9] For dynamical masses enclosed within the 3D half-light radius, Wolf et al. (2010) and Errani et al. (2018) give near-identical results. The derivation presented in the latter work, based on the projected virial theorem, guarantees that the results are independent of anisotropy in the velocity dispersion.

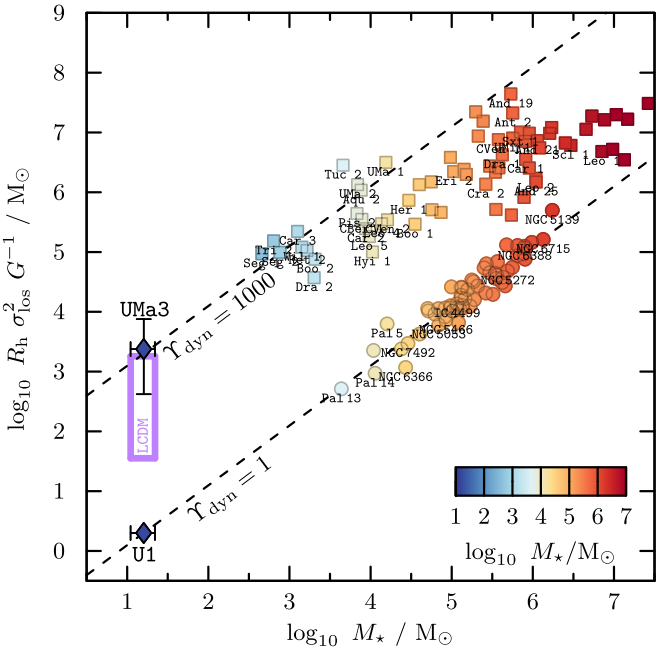

Figure 4. Dynamical mass, $R_{\rm h}\sigma^2_{\rm los}G^{-1}$, vs. stellar mass, $M_\star$, for Local Group dwarf galaxies (squares) and GCs (circles). The dashed diagonal lines indicate dynamical-to-stellar mass ratios of $\Upsilon_{\rm dyn} = 1$ and 1000, respectively (see Equation (8) for the definition). GCs are distributed with little scatter around the $\Upsilon_{\rm dyn} = 1$ line. Dwarf galaxies, whose dynamics are dominated by dark matter, lie well above that line. Taking its measured velocity dispersion at face value, UMa3 is located well within the LCDM prediction (the purple rectangle; see Section 3.2), whereas the SG model explored in Section 2, by construction, falls exactly on the $\Upsilon_{\rm dyn} = 1$ line. References for the data shown are listed in footnote 8.

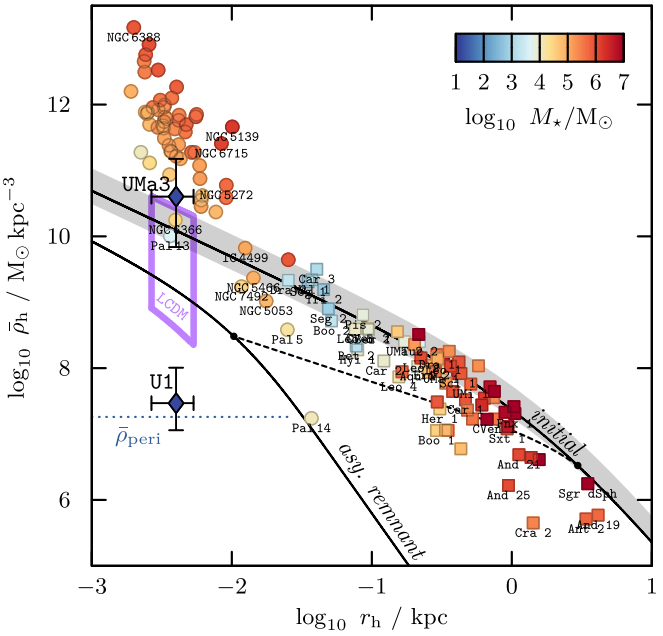

Figure 5. Mean density, $\bar{\rho}_{\rm h}$, enclosed within the 3D half-light radius, $r_{\rm h}$, for Local Group dwarf galaxies (squares) and GCs (filled circles), compared with UMa3/U1. The diamond labeled "U1" shows the mean density expected if UMa3/U1 is a fully self-gravitating stellar system without dark matter. The upper diamond labeled "UMa3"' corresponds to adopting the measured velocity dispersion of 1.9 km s^{-1}. A gray band shows the mean enclosed densities as a function of radius for LCDM (NFW) halos considered sufficiently massive to allow stars to form, taking into account the expected scatter in concentration (see the text for details). An example halo (labeled "initial") with a virial mass of $M_{\rm cr}^{z=2} \approx 9.5 \times 10^8\,M_\odot$, corresponding to the $z = 2$ hydrogen-cooling critical mass with average concentration, is shown in black. The dashed curve illustrates the "tidal track" tracing the evolution of the characteristic density $\bar{\rho}_{\rm mx} = \bar{\rho}(<r_{\rm mx})$ and size $r_{\rm mx}$ of an NFW halo as it is stripped by tides, with the black circles highlighting the initial and asymptotic values. The lower black curve corresponds to the asymptotic remnant of the "initial" model placed on the UMa3/U1 orbit.

We estimate the density of UMa3 by computing the dynamical mass enclosed within its 3D half-light radius using (see footnote 9)

$$M_{\rm dyn}(<r_{\rm h}) \approx 4\,R_{\rm h}\langle\sigma^2_{\rm los}\rangle G^{-1} = (1.0^{+2.1}_{-0.8}) \times 10^4\,M_\odot\,, \quad (9)$$

and dividing by the volume of a sphere of radius $r_{\rm h} = (4/3)R_{\rm h}$. If $\sigma_{\rm los} = 1.9^{+1.4}_{-1.1}$ km s^{-1}, this yields

$$\bar{\rho}_{\rm h} = (4^{+11}_{-3}) \times 10^{10}\,M_\odot\ {\rm kpc}^{-3}\,, \quad (10)$$

which is roughly $\sim$1000 times higher than the density of the SG model, and thus safe from tidal disruption. As shown by the blue diamond labeled "UMa3" in Figure 5, the mean density of UMa3 would in that case be comparable to that of some GCs, many of which are known to orbit the Galaxy on orbits with pericenters as small as or smaller than 13 kpc.

The mean density computed above would make UMa3 not only the faintest and smallest, but also the densest UFD ever detected, with important implications for both the mass of the CDM halo inhabited by UMa3 and for alternative models of dark matter. We address these issues next.

3.2. LCDM Expectations

In LCDM, galaxies form deep within the potential wells of dark matter halos (White & Rees 1978). The ability of hydrogen gas to cool efficiently in the presence of the cosmic UV background is expected to impose a minimum *critical* halo mass below which LCDM halos are not expected to be able to host luminous galaxies.

Benitez-Llambay & Frenk (2020) argue that, after reionization, the critical virial mass needed to enable star formation to proceed evolves with redshift z roughly as

$$M_{\rm cr}^z \approx (10^{10}M_\odot)[T/(3.2 \times 10^4\ {\rm K})]^{3/2}(1+z)^{-3/2}\,, \quad (11)$$

using a virial temperature of $T = 2 \times 10^4$ K. At redshift $z = 0$, the resulting critical mass equals $M_{\rm cr}^{z=0} \approx 4.9 \times 10^9\,M_\odot$.

At earlier redshifts, the critical mass was somewhat lower. The best-fitting isochrone for U1/UMa3 corresponds to a stellar age of $\gtrsim$11 Gyr (S24). Assuming Planck Collaboration et al. (2020) cosmological parameters, this corresponds roughly to a redshift of $z \sim 2$, which we shall adopt in what follows.

The cosmological simulations analyzed by Pereira-Wilson et al. (2023) confirm that stars first form in halos exceeding the critical mass given by Equation (11). We use their Figure 7 to estimate a range of halo masses for the potential progenitor halo of UMa3 (up to 0.5 dex above $M_{\rm cr}$) . Combining this with the $z = 2$ average NFW concentration ($\pm$0.15 dex scatter) from Ludlow et al. (2016), we obtain a range of mass profiles for UMa3, which we show as a gray band in Figure 5. The mean density profile of a halo with virial mass $M_{\rm cr}^{z=2} \approx 9.5 \times 10^8\,M_\odot$ is shown as a solid black curve within the gray band.

Figure 5 shows that UMa3's mass density is (for the assumed $\sigma_{\rm los}$) comfortably within the range expected for a galaxy inhabiting a cuspy NFW halo with mass close to critical.

Less massive NFW halos are less dense at all radii, and would therefore have difficulty matching UMa3's estimated density. For example, an LCDM "minihalo" with virial mass $10^6\,M_\odot$ at $z=0$ would have a mean density of $\approx 1.2\times10^9\,M_\odot\,\mathrm{kpc}^{-3}$ at $r\sim4$ pc, well below UMa3.

The high dark matter density estimated for UMa3 thus disfavors the possibility that it may have formed at the center of a minihalo and supports the view that luminous galaxies, no matter how faint, only form in halos near or above the critical virial mass of Benitez-Llambay & Frenk (2020) .

If UMa3 is indeed a "microgalaxy" (EP20) at the center of a cuspy NFW halo, we may use the results of EN21 and Errani et al. (2022) to predict its evolution under the influence of the Galactic tidal field.[10] The main result of their study is that tides gradually strip a halo, approaching an asymptotic state where the characteristic density of the bound remnant equals roughly $16\times\bar{\rho}_{\rm peri}$. The subhalo characteristic density evolves following a well-defined "tidal track" (Peñarrubia et al. 2008) until the asymptotic characteristic density has been reached. The bound remnant is well approximated by an "exponentially truncated" NFW profile (see EN21 for details).

The initial density profile of a halo of critical mass $M_{\rm cr}^{z=2}$ is shown by the solid black curve in Figure 5, labeled "initial". This halo has a circular velocity that peaks at $V_{\rm mx}=23\,\mathrm{km\,s^{-1}}$ at a radius $r_{\rm mx}=3.0$ kpc. Its characteristic mean density at $r_{\rm mx}$ equals $\bar{\rho}_{\rm mx}=3.3\times10^6\,M_\odot\,\mathrm{kpc}^{-3}$, shown as a black circle in Figure 5. The tidal track is shown by the dashed black curve, which stops once the asymptotic remnant density of $\bar{\rho}_{\rm mx}\approx16\times\bar{\rho}_{\rm peri}$ has been reached. An exponentially truncated NFW profile (the black curve labeled "asy. remnant") illustrates the final density profile of that halo on this orbit.

We emphasize that the asymptotic remnant properties depend on those of the initial NFW halo adopted. Choosing an initial halo with a higher characteristic initial density would lead to an asymptotic remnant whose mean density, at $r=4$ pc, is higher. It is clear from Figure 5 that although Galactic tides are expected to reduce the central dark matter density of a cuspy halo, a well-characterized bound remnant is predicted to survive, whose density at radii as small as 4 pc may be as high as $\sim10^{10}\,M_\odot\,\mathrm{kpc}^{-3}$.

The full range of dynamical masses and densities expected at that radius in LCDM (varying halo mass and concentration) is shown by the purple curves labeled "LCDM" in Figures 4 and 5, respectively. The corresponding range of velocity dispersions is $0.16\lesssim\sigma_{\rm los}/\mathrm{km\,s^{-1}}\lesssim1.5$, which is compatible with the current 10-member dispersion estimate of $\sigma_{\rm los}=1.9^{+1.4}_{-1.1}$ km s^{-1} (S24). We conclude that UMa3's properties are consistent with those expected from a microgalaxy deeply embedded at the center of a fairly massive, cuspy LCDM halo.

3.3. Consequences for Alternative Dark Matter Models

Although consistent with LCDM, the extreme properties of UMa3 inferred assuming that the 10-member velocity dispersion measurement holds ($\sigma_{\rm los}=1.9^{+1.4}_{-1.1}$ km s^{-1}) would be difficult to reconcile with alternative dark matter models that predict lower dark matter densities.

We begin by discussing UFDs in FDM models, where the density of a dark-matter-dominated UFD is thought to reflect the central density of the "solitonic core" that forms at the center of a halo made up of ultralight particles (Schive et al. 2014a, 2014b; Safarzadeh & Spergel 2020). Cosmological simulations of FDM halo formation find that the central density of the core, at redshift $z=0$, is given by (using Equations (3) and (7) in Schive et al. 2014b)

$$\rho_{\rm c0}\approx2.9\times10^6\,\frac{M_\odot}{\mathrm{kpc}^3}\left(\frac{m_\psi}{10^{-22}\,\mathrm{eV/c^2}}\right)^2\left(\frac{M_{\rm halo}}{10^9\,M_\odot}\right)^{4/3},\quad(12)$$

where m_ψ is the mass of the ultralight particle and $M_{\rm halo}$ is a measure of the halo virial mass.[11]

Attempts to fit the density profile of the "classical" dwarf spheroidal satellites of the Milky Way (like Fornax or Sculptor) with a solitonic core yield upper limits for m_ψ of order $10^{-22}\,\mathrm{eV\,c^{-2}}$ (Marsh & Pop 2015; González-Morales et al. 2017). This is mainly because the mean densities of Fornax and Sculptor are of order 10^7–$10^8\,M_\odot\,\mathrm{kpc}^{-3}$, consistent with Equation (12) for $M_{\rm halo}\sim10^{10}\,M_\odot$ and $m_\psi\sim10^{-22}\,\mathrm{eV}\,c^{-2}$.

Achieving a density as high as that estimated for UMa3 (i.e., $\sim4\times10^{10}\,M_\odot\,\mathrm{kpc}^{-3}$; see Equation (10)) would require the ultralight particle mass to be as large as $m_\psi\sim3\times10^{-21}\,\mathrm{eV}\,c^{-2}$ (or a halo mass as large as $M_{\rm halo}\sim10^{12}\,M_\odot$, which seems rather unlikely). This choice, however, would deny the main motivation for FDM: that the presumed kiloparsec-scale cores in dwarf galaxies suggested by some studies reflect the de Broglie wavelength of the ultralight particle (Goodman 2000; Hu et al. 2000; Hui et al. 2017; Ferreira 2021). Reconciling FDM with the high densities of observed UFDs has already been recognized as a difficult challenge to traditional FDM models (Burkert 2020; Safarzadeh & Spergel 2020), a challenge that would become much more severe if the high density of UMa3 is confirmed by future velocity dispersion measurements.

Finally, the estimated high density of UMa3 is also difficult to accommodate with the kiloparsec-size cores expected in SIDM models, at least for interaction cross sections of order $1\,\mathrm{cm^2\,g^{-1}}$ (see, e.g., Tulin & Yu 2018 and references therein). For this choice, collisions between particles erase the central cusp of a dark matter halo, creating a core with constant density that, on the scale of dwarf galaxies, does not exceed a few times $10^8\,M_\odot\,\mathrm{kpc}^{-3}$ (Zavala et al. 2013; Vogelsberger et al. 2014). Matching the high density of UMa3 (and, indeed, other UFDs) would require gravothermal "core collapse" to occur, raising the innermost dark matter densities to values as large as those predicted for cuspy LCDM halos and observed in UFDs (see, e.g., Hayashi et al. 2021; Silverman et al. 2023).

The timescale for core collapse, however, likely exceeds the age of the Universe for SIDM models with velocity-independent interaction cross sections (Zeng et al. 2022; though some authors argue that the core-collapse timescales may be shortened considerably by tidal effects—see Nishikawa et al. 2020). Further work is clearly needed to reconcile SIDM models with the high densities of UFDs in general, and of UMa3 in particular, should the current density estimate prove robust to binary stars.

[10] We compare the tidal evolution of UMa3 as predicted by the EN21 model against controlled N-body simulations in Appendix B.

[11] The definitions of the halo virial mass $M_{\rm halo}$ and virial radius in Schive et al. (2014b) are slightly different from the ones we use throughout this work (see footnote 5): at redshift $z=0$, the mean density enclosed within the virial radius equals ≈350 times the mean density of the Universe.

3.4. Annihilation Signals

The remarkably high density of $\bar{\rho}_{\rm h} \sim 4 \times 10^{10}\, M_\odot\, {\rm kpc}^{-3}$ (Equation (10)) combined with the heliocentric distance of only (10 ± 1)kpc (S24) render UMa3/U1 an interesting target for the study of potential signals of dark matter self-annihilation. The astrophysical component to the annihilation signal for velocity-independent annihiliation may be expressed through the J-factor (see, e.g., Walker et al. 2011), which for stellar tracers embedded in an NFW subhalo can be estimated from (see Equation (13) in Evans et al. 2016)

$$J \equiv \iint {\rm d}l{\rm d}\Omega\, \rho^2_{\rm NFW} \approx \frac{25}{8G^2}\frac{\sigma^4_{\rm los}\theta}{DR^2_{\rm h}} \sim 10^{21}\, \frac{{\rm GeV}^2/{\rm c}^4}{{\rm cm}^5}\,. \quad (13)$$

In the above equation, the integral is performed along the line of sight l over a solid angle $\Delta\Omega$, and D, $R_{\rm h}$, and $\sigma_{\rm los}$ are the heliocentric distance, projected half-light radius, and line-of-sight velocity dispersion of UMa3/U1, respectively. The angle θ limits the solid angle over which the integral is computed, and is chosen here to match the Fermi Large Area Telescope resolution at gigaelectronvolt scales, $\theta = 0.^\circ5$ (Ackermann et al. 2014). The J-factor of $\sim 10^{21}\, {\rm GeV}^2\, c^{-4}\, {\rm cm}^{-5}$ computed in Equation (13) takes the measured properties of UMa3/U1 at face value. Monte Carlo sampling of the measurement uncertainties yields a 16th–84th percentile range of $10^{19} \lesssim J/({\rm GeV}^2\, c^{-4}\, {\rm cm}^{-5}) \lesssim 10^{22}$ for the underlying distribution. Even when taking these large uncertainties into account, UMa3/U1 would be one of the "brightest" satellites of the Milky Way for potential annihilation signals, matching or exceeding the expected signal of all other known Milky Way dwarf spheroidal and ultrafaint satellites (see Table A2 in Pace & Strigari 2019).

4. Summary and Conclusions

UMa3/U1 is a recently discovered satellite of the Milky Way whose extreme properties offer unique insights into the formation process of some of the faintest objects in the Universe. It is by far the faintest satellite ever discovered: at $M_{\rm V} \approx +2.2$, it is $\sim$10 times fainter than the faintest confirmed ultrafaint dwarfs and $\sim$10 times fainter than the least luminous GC. It is also as small as some of the most compact GCs, with a projected half-mass radius of only $\sim$3 pc.

Taken at face value, the line-of-sight velocity dispersion computed from the radial velocities of 10 or 11 likely members suggests the presence of dark matter (which would confirm that UMa3/U1 is indeed a dwarf galaxy). However, the lack of repeat velocity measurements and the strong dependence of the measured dispersion on the inclusion of two specific member stars leave open the possibility that UMa3/U1 is actually a self-gravitating faint cluster of stars.

The main conclusions of our work are summarized below.

(1) The orbit of the system around the Milky Way is well characterized, with a pericentric distance of only $\approx$13 kpc, an apocentric distance of $\approx$30 kpc, and a radial orbital time of $\approx$0.4 Gyr. We use N-body simulations to show that, taking its observed size and stellar mass at face value, UMa3/U1 cannot survive for much longer than a single orbit if self-gravitating. Either UMa3/U1 is a GC remnant observed at a remarkably fine-tuned point in time or it is indeed a galaxy that has survived tidal disruption because of the stabilizing effect of dark matter.

(2) The simulations do rule out the possibility that "tidal stirring" may have enhanced the observed $\sigma_{\rm los}$ to values as high as a few kilometers per second. The models predict that, if self-gravitating, UMa3/U1 should be surrounded by a stream of tidally stripped stars, which should be searched for with high priority.

We conclude that (1) and (2) strongly support the view that UMa3/U1 is a dark-matter-dominated "microgalaxy," indeed the faintest, or "darkest," galaxy ever discovered.

(3) If the $\sigma_{\rm los} = 1.9^{+1.4}_{-1.1}$ km s^{-1} estimated using the 10 most likely member stars is correct, then the mean dark matter density for UMa3/U1 would be $\approx 4 \times 10^{10}\, M_\odot\, {\rm kpc}^{-3}$ within its 3D half-light radius of $\sim$4 pc. This makes UMa3/U1 the densest ultrafaint galaxy known, a result that suggests that UMa3/U1 formed at the very center of a fairly massive ($\sim 10^9$–$10^{10}\, M_\odot$) cuspy CDM halo, whose innermost regions should be able to survive the strong tidal field of the Galaxy for a Hubble time. This in turn implies a relatively high halo mass threshold for luminous galaxy formation in LCDM, as advocated by the "critical" mass model of Benitez-Llambay & Frenk (2020).

(4) If confirmed, the high dark matter density estimated for UMa3/U1 would have strong implications for alternative dark matter models. In the case of FDM, identifying it with the central density of the "solitonic core" yields an estimate for the mass of the ultralight particle of $\sim 3 \times 10^{-21}$ eV, more than 1 order of magnitude higher than the 10^{-22} eV upper limits inferred in previous work (Marsh & Pop 2015; González-Morales et al. 2017). This inconsistency casts doubt on the ground motivation for FDM models, which, if confirmed, would require a reevaluation of the model.

(5) Such a high dark matter density would also place strong constraints on SIDM models, where the dense halo cusps are eroded by collisional effects, leading to a substantial reduction of the dark matter central densities compared to LCDM. In the context of SIDM, UMa3/U1's central density can only be reproduced in systems that have undergone gravothermal "core collapse," placing stringent constraints on the allowed values of the collisional cross section.

Our models show that accurate and extremely precise dispersion estimates are crucial to differentiating between UMa3/U1 being a dark-matter-dominated "microgalaxy" or an extremely faint self-gravitating star cluster. If the current estimate of UMa3's dynamical density is confirmed by future observations, it would not only confirm UMa3 as the "darkest" galaxy discovered to date, but it would also highlight that the predictions of LCDM seem to hold down to the faintest end of the galaxy luminosity function.

Acknowledgments

The authors would like to thank W. Cerny, T. S. Li and M. G. Walker for their helpful comments on the draft. R.E. acknowledges support from the European Research Council (ERC) under the European Union's Horizon 2020 research and

innovation program (grant agreement No. 834148) and from the National Science Foundation (NSF) grant AST-2206046.

Appendix A
Tidal Mass Loss on Different Orbits

The tidal evolution and potential disruption of UMa3/U1 depend on its orbit. In Section 2, we use *N*-body simulations to study the tidal disruption of UMa3/U1 in the EP20 Milky Way potential, taking the observed position of UMa3/U1 at face value. In the following, we will extend the analysis to include a second potential and account for observational uncertainties in the present position and velocity of UMa3/U1.

The axisymmetric EP20 Milky Way potential has a circular velocity of $V_c(R_\odot) = 240\,\mathrm{km\,s^{-1}}$ at the solar radius. As a second example potential, we use the Bovy (2015) model with $V_c(R_\odot) = 220\,\mathrm{km\,s^{-1}}$. These two potential models nicely bracket the rotation curve measured by Eilers et al. (2019). We integrate point-mass orbits in these two potentials. The initial conditions are obtained by drawing Monte Carlo samples from the distribution of measured distance, radial velocity, and proper motions of UMa3/U1, with uncertainties as listed in S24. For the EP20 potential, we obtain pericenter and apocenter estimates of $r_{\rm peri} = (13 \pm 1)$kpc and $r_{\rm apo} = (30^{+4}_{-3})$kpc. For the case of the Bovy (2015) potential, our pericenter estimate is virtually identical, whereas for the apocenter, we find $r_{\rm apo} = (38^{+6}_{-5})$kpc. The uncertainties quoted correspond to the 16th and 84th percentiles of the underlying distribution.

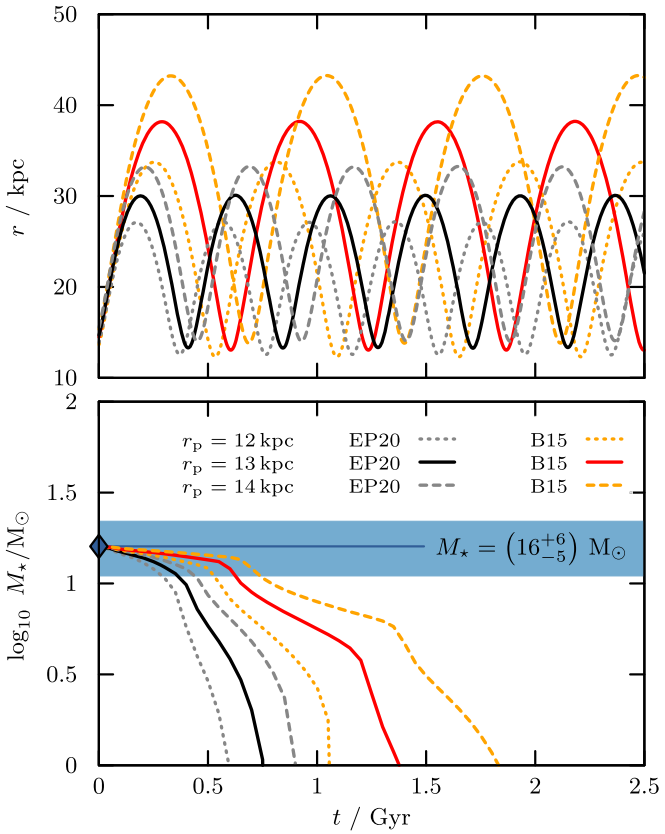

Figure 6. Top panel: galactocentric distance of UMa3/U1 as a function of time, obtained by forward integrating orbits in the EP20 (black curves) and Bovy (2015; red curves) potentials. The solid curves take the current position and velocity of UMa3/U1 at face value. The dotted and dashed lines correspond to orbits representative of the 16th and 84th percentiles of the underlying distribution of measurement uncertainties. Bottom panel: the evolution of the bound mass of SG *N*-body models evolved on the orbits shown above. In all cases, the SG models disrupt within a few pericenter passages.

The top panel of Figure 6 shows the galactocentric distance of UMa3/U1 as a function of time for three orbits in the EP20 potential and three orbits in the Bovy (2015) potential. The solid curves show the orbit obtained by taking the measured position and velocity of UMa3/U1 at face value, while the dotted and dashed curves show orbits representative of the 16th and 84th percentiles of the underlying distribution.

For each of the orbits shown in the top panel of Figure 6, we evolve an *N*-body model of UMa3/U1 forward in time, using the same setup as in Section 2. The initial stellar mass and half-light radius are chosen to match the currently observed values of $M_\star = 16\,M_\odot$ and $R_{\rm h} = 3$ pc. We show the evolution of the bound mass for each of these *N*-body models in the bottom panel of Figure 6. All models disrupt within the next few pericenter passages, showing that the results of Section 2 are fairly insensitive to the choice of the Milky Way potential, and fairly robust within the estimated uncertainties of the observed position and velocity of UMa3/U1.

Appendix B
Supplementary Dark-matter-only *N*-body Simulations

In Section 3, we discuss the observable consequences for a scenario where UMa3/U1 is embedded in a dark matter subhalo. Our analysis makes use of the empirical findings of EN21, which suggest that tidally stripped NFW halos converge toward a stable asymptotic remnant state, where the characteristic density of the subhalo is determined by the mean density of the host at pericenter. The model of EN21 assumes a spherical, isothermal host potential. The combined mass distribution of the halo, bulge, and disk in the inner regions of the Milky Way is not spherical, however, but more appropriately approximated by an axisymmetric model. Using *N*-body simulations, we now aim to test to what extent the tidal evolution of a dark matter subhalo on the orbit of UMa3/U1 depends on the geometry of the underlying potential.

We place two NFW *N*-body subhalo models on orbits with pericenter and apocenter matching those of UMa3/U1, and evolve these models in (1) the axisymmetric EP20 potential and (2) a spherical isothermal potential with a constant circular velocity of $V_c = 240\,\mathrm{km\,s^{-1}}$. The *N*-body subhalo models are chosen to have initial properties identical to those of the $z = 2$ hydrogen cooling limit halo of Figure 5, and $N = 10^7$ particles. We generate the models using the same code as in Section 2 (see footnote 7), and evolve the models using the particle mesh code SUPERBOX (Fellhauer et al. 2000), adopting a spatial resolution of $\Delta x \approx 20$ pc for the highest-resolving grid.

The results of the experiment are shown in Figure 7, where we confront the time evolution of the subhalo structural parameters $r_{\rm mx}$, $V_{\rm mx}$ measured in the two *N*-body models against those computed using the EN21 model. For the first $\sim$2 Gyr of tidal evolution, both *N*-body models are in good agreement with EN21. The gray shaded area in Figure 7 shows the region of parameter space where the number of *N*-body particles ($N_{\rm mx} \leqslant 3000$) and/or the spatial resolution of the simulation ($r_{\rm mx} \leqslant 8\Delta x$) are insufficient to reliably model the tidal evolution of the subhalo (see Appendix A in EN21 for a convergence study). Indeed, in the gray shaded region, the evolution of the *N*-body models diverges from the EN21 track, and both models *artificially* disrupt after $\sim$5 Gyr of evolution. The EN21 model instead predicts an evolution toward a stable

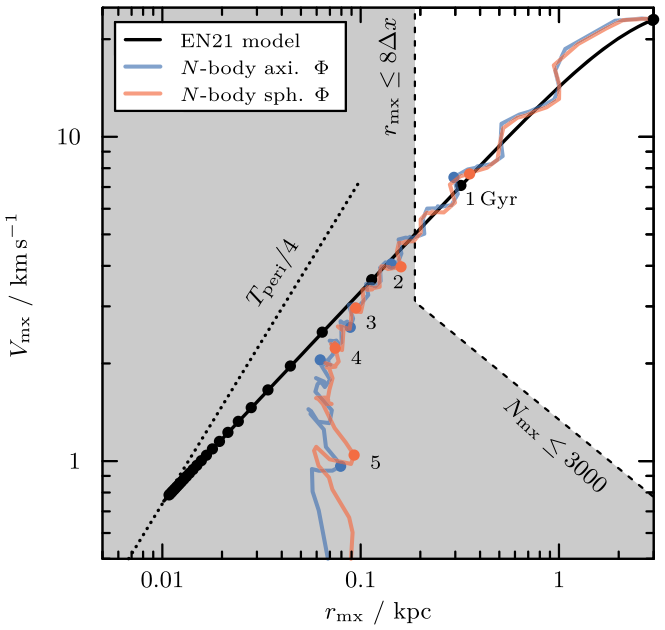

Figure 7. Tidal evolution of characteristic size $r_{\rm mx}$ and velocity $V_{\rm mx}$ for an NFW subhalo on the orbit of UMa3/U1. The initial values ($r_{\rm mx0} = 3$ kpc, $V_{\rm mx0} = 23$ km s^{-1}) are identical to the subhalo model discussed in Section 3. A black solid curve shows the evolution computed using the EN21 model, while the blue and red curves correspond to *N*-body models evolved in an axisymmetric and a spherical host potential, respectively. The gray shaded area shows the parameter space where the *N*-body models are likely affected by insufficient particle numbers ($N_{\rm mx} \leqslant 3000$) and/or spatial resolution ($r_{\rm mx} \leqslant 8\Delta x$). Both *N*-body models disrupt *artificially* after ≈5 Gyr, whereas the EN21 model predicts an evolution toward a stable remnant state.

remnant state. The filled circles along the evolutionary track are spaced by 1 Gyr and show that the remnant state is approached asymptotically, with tidal evolution gradually slowing down as the remnant state is approached.

Remarkably, the tidal evolution of the *N*-body model evolved in the axisymmetric potential is near identical to the one evolved in the spherical potential. For the orbit of UMa3/U1, the detailed shape of the potential hence seems to have negligible impact on the tidal evolution of a dark matter subhalo.

ORCID iDs

Julio F. Navarro https://orcid.org/0000-0003-3862-5076
Simon E. T. Smith https://orcid.org/0000-0002-6946-8280
Alan W. McConnachie https://orcid.org/0000-0003-4666-6564

References

Ackermann, M., Albert, A., Anderson, B., et al. 2014, PhRvD, 89, 042001
Amorisco, N. C. 2021, arXiv:2111.01148
Amorisco, N. C., & Evans, N. W. 2012, MNRAS, 419, 184
Balberg, S., Shapiro, S. L., & Inagaki, S. 2002, ApJ, 568, 475
Balbinot, E., Santiago, B. X., da Costa, L., et al. 2013, ApJ, 767, 101
Battaglia, G., & Nipoti, C. 2022, NatAs, 6, 659
Baumgardt, H., Côté, P., Hilker, M., et al. 2009, MNRAS, 396, 2051
Belokurov, V., Walker, M. G., Evans, N. W., et al. 2009, MNRAS, 397, 1748
Benitez-Llambay, A., & Frenk, C. 2020, MNRAS, 498, 4887
Binney, J., & Tremaine, S. 1987, Galactic Dynamics (Princeton, NJ: Princeton Univ. Press)
Bode, P., Ostriker, J. P., & Turok, N. 2001, ApJ, 556, 93
Bovy, J. 2015, ApJS, 216, 29
Bruce, J., Li, T. S., Pace, A. B., et al. 2023, ApJ, 950, 167
Bullock, J. S., & Boylan-Kolchin, M. 2017, ARA&A, 55, 343
Burkert, A. 2020, ApJ, 904, 161
Cerny, W., Drlica-Wagner, A., Li, T. S., et al. 2023a, ApJL, 953, L21
Cerny, W., Martínez-Vázquez, C. E., Drlica-Wagner, A., et al. 2023b, ApJ, 953, 1
Chiti, A., Frebel, A., Simon, J. D., et al. 2021, NatAs, 5, 392
Colín, P., Avila-Reese, V., Valenzuela, O., & Firmani, C. 2002, ApJ, 581, 777
Collins, M. L. M., Read, J. I., Ibata, R. A., et al. 2021, MNRAS, 505, 5686
Collins, M. L. M., Tollerud, E. J., Rich, R. M., et al. 2020, MNRAS, 491, 3496
Correa, C. A., Schaller, M., Ploeckinger, S., et al. 2022, MNRAS, 517, 3045
Drlica-Wagner, A., Bechtol, K., Rykoff, E. S., et al. 2015, ApJ, 813, 109
Efstathiou, G. 1992, MNRAS, 256, 43P
Eilers, A.-C., Hogg, D. W., Rix, H.-W., & Ness, M. K. 2019, ApJ, 871, 120
Errani, R., & Navarro, J. F. 2021, MNRAS, 505, 18
Errani, R., Navarro, J. F., Ibata, R., & Peñarrubia, J. 2022, MNRAS, 511, 6001
Errani, R., Navarro, J. F., Peñarrubia, J., Famaey, B., & Ibata, R. 2023, MNRAS, 519, 384
Errani, R., & Peñarrubia, J. 2020, MNRAS, 491, 4591
Errani, R., Peñarrubia, J., & Walker, M. G. 2018, MNRAS, 481, 5073
Evans, N. W., Sanders, J. L., & Geringer-Sameth, A. 2016, PhRvD, 93, 103512
Fattahi, A., Navarro, J. F., Frenk, C. S., et al. 2018, MNRAS, 476, 3816
Fellhauer, M., Kroupa, P., Baumgardt, H., et al. 2000, NewA, 5, 305
Ferreira, E. G. M. 2021, A&ARv, 29, 7
Ferrero, I., Abadi, M. G., Navarro, J. F., Sales, L. V., & Gurovich, S. 2012, MNRAS, 425, 2817
Frebel, A., & Norris, J. E. 2015, ARA&A, 53, 631
Geha, M., Willman, B., Simon, J. D., et al. 2009, ApJ, 692, 1464
Gieles, M., Erkal, D., Antonini, F., Balbinot, E., & Peñarrubia, J. 2021, NatAs, 5, 957
Gnedin, N. Y. 2000, ApJ, 542, 535
González-Morales, A. X., Marsh, D. J. E., Peñarrubia, J., & Ureña-López, L. A. 2017, MNRAS, 472, 1346
Goodman, J. 2000, NewA, 5, 103
Hansen, T. T., Simon, J. D., Marshall, J. L., et al. 2017, ApJ, 838, 44
Harris, W. E. 1996, AJ, 112, 1487
Hayashi, K., Ibe, M., Kobayashi, S., Nakayama, Y., & Shirai, S. 2021, PhRvD, 103, 023017
Hernquist, L. 1990, ApJ, 356, 359
Hilker, M. 2006, A&A, 448, 171
Hu, W., Barkana, R., & Gruzinov, A. 2000, PhRvL, 85, 1158
Huang, Y., Liu, X. W., Yuan, H. B., et al. 2016, MNRAS, 463, 2623
Hui, L., Ostriker, J. P., Tremaine, S., & Witten, E. 2017, PhRvD, 95, 043541
Inman, R. T., & Carney, B. W. 1987, AJ, 93, 1166
Ji, A. P., Koposov, S. E., Li, T. S., et al. 2021, ApJ, 921, 32
Ji, A. P., Simon, J. D., Frebel, A., Venn, K. A., & Hansen, T. T. 2019, ApJ, 870, 83
Jordi, K., Grebel, E. K., Hilker, M., et al. 2009, AJ, 137, 4586
Koposov, S., Belokurov, V., Evans, N. W., et al. 2008, ApJ, 686, 279
Koposov, S., de Jong, J. T. A., Belokurov, V., et al. 2007, ApJ, 669, 337
Kuzma, P. B., Da Costa, G. S., Keller, S. C., & Maunder, E. 2015, MNRAS, 446, 3297
Laporte, C. F. P., Agnello, A., & Navarro, J. F. 2019, MNRAS, 484, 245
Li, H., Hammer, F., Babusiaux, C., et al. 2021, ApJ, 916, 8
Lovell, M. R., Frenk, C. S., Eke, V. R., et al. 2014, MNRAS, 439, 300
Ludlow, A. D., Bose, S., Angulo, R. E., et al. 2016, MNRAS, 460, 1214
Marsh, D. J. E., & Pop, A.-R. 2015, MNRAS, 451, 2479
Marshall, J. L., Hansen, T., Simon, J. D., et al. 2019, ApJ, 882, 177
Martin, N. F., Geha, M., Ibata, R. A., et al. 2016, MNRAS, 458, L59
Martin, N. F., Ibata, R. A., McConnachie, A. W., et al. 2013, ApJ, 776, 80
Mau, S., Cerny, W., Pace, A. B., et al. 2020, ApJ, 890, 136
McConnachie, A. W. 2012, AJ, 144, 4
McConnachie, A. W., & Côté, P. 2010, ApJL, 722, L209
McConnachie, A. W., & Venn, K. A. 2020a, RNAAS, 4, 229
McConnachie, A. W., & Venn, K. A. 2020b, AJ, 160, 124
McMillan, P. J. 2011, MNRAS, 414, 2446
Minor, Q. E., Martinez, G., Bullock, J., Kaplinghat, M., & Trainor, R. 2010, ApJ, 721, 1142
Miyamoto, M., & Nagai, R. 1975, PASJ, 27, 533
Muñoz, R. R., Geha, M., Côté, P., et al. 2012, ApJL, 753, L15
Nadler, E. O., Drlica-Wagner, A., Bechtol, K., et al. 2021, PhRvL, 126, 091101
Navarro, J. F., Frenk, C. S., & White, S. D. M. 1996, ApJ, 462, 563
Navarro, J. F., Frenk, C. S., & White, S. D. M. 1997, ApJ, 490, 493
Nishikawa, H., Boddy, K. K., & Kaplinghat, M. 2020, PhRvD, 101, 063009
Pace, A. B., & Li, T. S. 2019, ApJ, 875, 77
Pace, A. B., & Strigari, L. E. 2019, MNRAS, 482, 3480

Peñarrubia, J., Benson, A. J., Walker, M. G., et al. 2010, MNRAS, 406, 1290
Peñarrubia, J., Navarro, J. F., & McConnachie, A. W. 2008, ApJ, 673, 226
Peñarrubia, J., Pontzen, A., Walker, M. G., & Koposov, S. E. 2012, ApJL, 759, L42
Pereira-Wilson, M., Navarro, J. F., Benítez-Llambay, A., & Santos-Santos, I. 2023, MNRAS, 519, 1425
Planck Collaboration, Aghanim, N., Akrami, Y., et al. 2020, A&A, 641, A6
Quinn, T., Katz, N., & Efstathiou, G. 1996, MNRAS, 278, L49
Safarzadeh, M., & Spergel, D. N. 2020, ApJ, 893, 21
Sales, L. V., Wetzel, A., & Fattahi, A. 2022, NatAs, 6, 897
Schive, H.-Y., Chiueh, T., & Broadhurst, T. 2014a, NatPh, 10, 496
Schive, H.-Y., Liao, M.-H., Woo, T.-P., et al. 2014b, PhRvL, 113, 261302
Schönrich, R., Binney, J., & Dehnen, W. 2010, MNRAS, 403, 1829
Silverman, M., Bullock, J. S., Kaplinghat, M., Robles, V. H., & Valli, M. 2023, MNRAS, 518, 2418
Simon, J. D. 2018, ApJ, 863, 89
Simon, J. D. 2019, ARA&A, 57, 375
Simon, J. D., & Geha, M. 2007, ApJ, 670, 313
Smith, S. E. T., Cerny, W., Hayes, C., et al. 2024, ApJ, 961, 92
Spitzer, L. 1987, Dynamical Evolution of Globular Clusters (Princeton, NJ: Princeton Univ. Press)
Spurzem, R., & Kamlah, A. 2023, LRCA, 9, 3
Taibi, S., Battaglia, G., Rejkuba, M., et al. 2020, A&A, 635, A152
Torrealba, G., Belokurov, V., & Koposov, S. E. 2019, MNRAS, 484, 2181
Tulin, S., & Yu, H.-B. 2018, PhR, 730, 1
Turner, H. C., Lovell, M. R., Zavala, J., & Vogelsberger, M. 2021, MNRAS, 505, 5327
Vogelsberger, M., Zavala, J., Simpson, C., & Jenkins, A. 2014, MNRAS, 444, 3684
Walker, M. G., Combet, C., Hinton, J. A., Maurin, D., & Wilkinson, M. I. 2011, ApJL, 733, L46
Walsh, S. M., Willman, B., & Jerjen, H. 2009, AJ, 137, 450
White, S. D. M., & Rees, M. J. 1978, MNRAS, 183, 341
Willman, B., & Strader, J. 2012, AJ, 144, 76
Wolf, J., Martinez, G. D., Bullock, J. S., et al. 2010, MNRAS, 406, 1220
Woo, J., Courteau, S., & Dekel, A. 2008, MNRAS, 390, 1453
Zavala, J., Vogelsberger, M., & Walker, M. G. 2013, MNRAS, 431, L20
Zeng, Z. C., Peter, A. H. G., Du, X., et al. 2022, MNRAS, 513, 4845
Zeng, Z. C., Peter, A. H. G., Du, X., et al. 2023, arXiv:2310.09910